NASA Technical Paper 1014

An Ultraviolet Video Technique for Visualization of Stack Plumes and for Measuring Sulfur Dioxide Concentration and Effluent Velocity

Reginald J. Exton

SEPTEMBER 1977

NASA

NASA Technical Paper 1014

An Ultraviolet Video Technique for Visualization of Stack Plumes and for Measuring Sulfur Dioxide Concentration and Effluent Velocity

Reginald J. Exton

Langley Research Center
Hampton, Virginia

National Aeronautics
and Space Administration

**Scientific and Technical
Information Office**

1977

SUMMARY

Absorption spectroscopy utilizing a video sensing technique has been investigated as a means of visualizing SO_2 in power plant stack plumes and for measuring SO_2 concentration and effluent velocity in these plumes. The absorption of SO_2 is measured in the ultraviolet region by using the sky (scattered sunlight) as a background source. An additional spectral channel, adjacent to the SO_2 band system, is used to correct for particulate scattering encountered in coal-fired power plant plumes. The video system also tracks fluctuations in the SO_2 concentration which leads to the determination of an eddy convection velocity. Field measurements were performed to show that the eddy convection velocity is proportional to the average in-stack velocity and to empirically determine their relationship. It was concluded that the video absorption technique is an attractive method for remotely determining both SO_2 concentration and plume velocity with the same instrument.

INTRODUCTION

The regulation of air pollution by controlling the emissions at their source is a primary task of the Environmental Protection Agency (EPA). Pursuant to the Clean Air Act, standards of performance for new stationary sources, such as coal- and oil-fired power plants, have been set forth (ref. 1) and performance specifications for continuous, stationary-source monitoring systems have also been outlined (ref. 2). The standards in reference 1 include emission limits for one or more of four pollutants (particulate matter, sulfur dioxide, nitrogen oxides, and sulfuric acid mist) for each source category. In addition to the standards, reference 1 describes specific sampling techniques and analysis methods for in-stack monitoring. Method 2 describes the apparatus and test procedure for the determination of stack gas velocity, whereas method 6 describes the test procedures for the determination of sulfur dioxide emissions. These methods are difficult and time-consuming in practice and usually require that special access ports be installed in the facility. In addition, the methods are not suitable for spot checks or general surveillance, and it is, therefore, desirable to develop remote methods of sensing these pollutants at the stack lip. Among the sophisticated remote techniques presently being developed are laser backscatter for opacity (ref. 3), infrared spectral emission (ref. 4), correlation spectroscopy (ref. 5), and differential absorption lidar (ref. 6) for gases and laser doppler velocimetry (LDV) (ref. 7) for effluent velocity.

An earlier paper (ref. 8) described a simple, solar radiometer for remotely measuring the plume opacity and the sulfur dioxide concentration. A major disadvantage of the solar radiometer, however, is the requirement that the Sun be viewable behind the plume. Physical constraints such as plant location, stack height, and surrounding terrain often restrict the use of the radiometer to a few observing positions or to a limited viewing time.

The technique described in this paper uses the daytime sky as a background and thus circumvents the viewing constraints encountered with the solar radiometer. In addition, ultraviolet video techniques are employed which allow visualization of the otherwise invisible plume. Concentration measurements are made by measuring the sky radiance on either side of the plume and through the center of the plume just above the stack lip. These measurements, made within the absorption band system of sulfur dioxide, can be related to the gaseous absorption if the effects of particulate attenuation and scattering can be assessed. For this latter purpose, an adjacent spectral channel is employed which is located outside of the sulfur dioxide band system. Finally, the visualization of the sulfur dioxide plume also allows a measurement of the effluent velocity by tracking fluctuations (turbulence) in the sulfur dioxide concentration.

The author would like to express his appreciation to the Environmental Science Research Laboratory of EPA for their cooperation in conducting this program and, in particular, to Dr. William F. Hergit of the Emission Measurements and Characterization Division for his continued interest and assistance in field testing of the system.

SYMBOLS

E	emission rate of sulfur dioxide, kg/hr
I_o	background intensity used in laboratory absorption measurements, arbitrary units
k	Boltzmann's constant, 1.38×10^{-23} J/K
L	path length, m
L_o	stack lip diameter, m
N	total number density of molecules, m^{-3}
n	number density of absorbers, m^{-3}
p	partial pressure, atm
p_o	partial pressure at T_o, atm
p_t	total pressure, atm (1 atm = 101.3 kN/m^2 = 760 torr)
R_o	background sky radiance, arbitrary units
R_1	ambient sky radiance, arbitrary units
R_2	plume radiance as seen by observer, $\tau_G \tau_p R_o + \tau_g \sigma_p R_1 + \delta$, arbitrary units
R_3	background radiance as seen by observer, $R_o + \delta$, arbitrary units

T temperature of plume, K

T_o temperature of calibration cells, K

t mean time for an eddy to propagate distance X, sec

V effluent velocity, m/sec

V_c eddy convection velocity, m/sec

X separation of video sensing points in flow, m

Z concentration of absorbers, ppm

α absorption coefficient, $(cm\text{-}atm)^{-1}$

δ path radiance from plume to observer, arbitrary units

θ viewing angle of observer

λ wavelength, nm

ρ radiance ratio, R_2/R_3

Σ ratio of scattered ambient sky radiance to background sky radiance, $\frac{\sigma_p R_1}{R_o}$

σ_p fraction of ambient sky radiance which is scattered by particulates toward observer

τ_G transmittance of absorbing gas for background sky radiance

τ_g effective transmittance of absorbing gas for ambient sky radiance

τ_p transmittance of particulates

Superscripts:

A denotes spectral quantities within SO_2 band system

B denotes spectral quantities adjacent to SO_2 band system

FACTORS AFFECTING PLUME RADIANCE

The use of the Sun directly as a background source simplified the analysis of the solar radiometer data (ref. 8). The attenuation measurements could be easily interpreted in terms of particulate opacity and gaseous absorption. The use of the sky as a background is more complex since the sky is a diffuse source of scattered sunlight, and the ambient sky radiance scattered by the

particulates in a plume can be a significant factor relative to the background sky radiance. Thus, the observer not only sees a plume having a radiance contribution from the sky background, but also has to contend with the scattered light originating from the ambient sky. Direct scatter from the Sun also contributes to the scattered plume radiance, but for zenith angles greater than 30^{o}, the ambient sky irradiance incident on the plume predominates over the direct solar irradiance (ref. 9). Finally, since the observer and target are embedded in the ambient scattering medium, the path radiance between them will also have to be taken into account.

The factors which affect the plume radiance as it occurs in coal-fired power plants are considered in this section. The factors discussed generally apply to other facilities such as oil-fired power plants and sulfuric acid plants if particulate emissions are neglected. For the path lengths encountered and concentrations expected, the pollutants listed are the only ones which will appreciably affect the plume radiance in the near ultraviolet and visible regions.

Particulates

In coal-fired plants, the visual appearance of plumes is primarily controlled by the particulate emissions. The particulates not only affect the plume transmittance, but also act as scattering sites for other ambient sky radiance. The particulate opacity ($1 - \tau_p$) depends on the size, number, shape, and complex refractive index of the particles as well as on the wavelength of the incident light (ref. 10). The detailed manner in which the particulates affect the plume transmittance depends on the oscillatory behavior in the extinction coefficient encountered for individual particles. It is found, however, that the normal polydispersed distribution of particle sizes found in stack emissions and the use of broad band light have a considerable smoothing effect on the extinction coefficient with the result that the transmittance exhibits only a weak dependence on the wavelength employed (refs. 2 and 10). This fact will be especially useful in assessing the particulate effects on a measurement of gas concentration.

Nitrogen Dioxide

The nitrogen dioxide component of the NO_x emitted exhibits absorption over a wide spectral range in the visible and near ultraviolet (ref. 11) as shown in figure 1. The absorption peaks at about 400 nm and has a half-power breadth of approximately 150 nm. A dimer (N_2O_4) exists which exhibits absorption below 400 nm (a peak at 350 nm) but is expected to be only a small percentage of the NO_2 at the temperatures encountered in typical stack-plume conditions. In-stack sampling indicates that most of the NO_x is emitted as NO with an upper limit for NO_2 as 10 to 20 ppm. Thus, the attenuation due to NO_2 will not significantly affect the plume radiance in the near ultraviolet. Absorption bands of NO are also situated in the ultraviolet but are not amenable to passive absorption techniques because of the stratospheric ozone cutoff.

Sulfur Dioxide

The pollutant sulfur dioxide is one of the prime concerns, particularly in coal-fired plants, where the burning of high-sulfur-content coal has come under careful scrutiny. A strong band system of SO_2 exists just at the stratospheric ozone cutoff shown in figure 1. Another weaker band system exists, centered at about 370 nm, which will not result in any measurable attenuation for the path lengths encountered (ref. 12). Sulfur dioxide concentrations in coal-fired plants are typically in the range 500 to 1500 ppm. Over this range, it is easy to measure the sulfur dioxide concentration if a correction for particulate attenuation and scattering effects can be obtained.

The transmittance τ_G through a gas, such as SO_2, is given by

$$\tau_G = e^{-\alpha p_o L} \tag{1}$$

where α is the spectral absorption coefficient, p_o is the partial pressure of the absorbers at temperature T_o, and L is the path length through the sample. For stack exit conditions at temperature T,

$$\left.\begin{aligned} p &= nkT \\ p_t &= NkT \approx 1 \text{ atm } (101.3 \text{ kN/m}^2) \end{aligned}\right\} \tag{2}$$

where n is the number density of absorbers, N is the total number density of molecules, and p_t is the total pressure. The concentration of absorbers in parts per million Z is given by

$$\frac{Z}{10^6} = \frac{n}{N} = \frac{p}{p_t} \tag{3}$$

Hence, the transmittance of the gas becomes

$$\tau_G = e^{-\frac{\alpha p_t T_o}{10^6}\frac{ZL}{T}} \tag{4}$$

TECHNIQUE

Concentration

A gas concentration measurement requires a determination of the gas transmittance τ_G as given in equation (4). The desired quantity τ_G, however, is masked by the particulate transmittance τ_P, and by the radiance scattered by the particulates. Figure 2 illustrates the contributions to the plume radiance R_2 ($R_2 = \tau_G\tau_P R_o + \tau_g\sigma_P R_1 + \delta$) due to the background sky radiance R_o, the ambient sky radiance R_1, and the path radiance δ between the plume and the observer. The first term in R_2 represents the effects of the gas transmittance τ_G and the particulate transmittance τ_P on the background radiance. The second term adds the effects of the ambient sky radiance that is scattered toward the observer. In this term, σ_P represents the fraction of the ambient sky radiance which is scattered toward the observer, whereas τ_g represents an effective plume gas transmittance for the ambient sky radiance. The background radiance as seen by the observer R_3 is just the sum of the background sky radiance R_o plus the path radiance from the plume to the observer δ.

In practice, a radiance ratio $\rho = R_2/R_3$ is made between the plume radiance and the background radiance as seen by the observer. This radiance ratio is measured in a spectral channel within the SO_2 band system ρ^B and also in an adjacent channel ρ^A in order to assess the effects of particulate attenuation and scattering. Channel A is chosen outside the SO_2 band system so that no gas transmittance terms are involved. These radiance ratios are given as follows:

$$\rho^B = \frac{R_2^B}{R_3^B} = \frac{\tau_G\tau_P R_o^B + \tau_g\sigma_P^B R_1^B + \delta^B}{R_o^B + \delta^B} \tag{5}$$

$$\rho^A = \frac{R_2^A}{R_3^A} = \frac{\tau_P R_o^A + \sigma_p^A R_1^A + \delta^A}{R_o^A + \delta^A} \tag{6}$$

By zeroing the instrumentation while observing a black target located at the stack, the effect of the path radiance δ can be suppressed to yield

$$\rho^B = \tau_G\tau_P + \tau_g\Sigma^B \tag{7}$$

$$\rho^A = \tau_P + \Sigma^A \tag{8}$$

with

$$\Sigma^B = \sigma_p{}^B \frac{R_1{}^B}{R_o{}^B}$$

and

$$\Sigma^A = \sigma_p{}^A \frac{R_1{}^A}{R_o{}^A}$$

where Σ represents the ratio of scattered ambient sky radiance to the background sky radiance. Equation (8) illustrates the effect that scattering can have on plume visibility. In this equation, an increase in opacity (τ_p decreasing) is normally accompanied by an increase in scattering, represented by Σ. These effects, therefore, tend to compensate for one another, and often render the plume invisible to the eye even though the opacity may be significant.

Assuming that the particulate scattering is the same for the two neighboring spectral channels $\left(\sigma_p{}^A = \sigma_p{}^B\right)$ and that the ratio of the ambient sky radiance R_1 to the background sky radiance R_o is a constant results in

$$\Sigma^A > \tau_g \Sigma^B \tag{9}$$

which states that the scattering effects observed in channel B are further reduced relative to those in channel A by the effective gas transmittance τ_g. Solving for τ_G in equation (7) and substituting Σ^A for $\tau_g \Sigma^B$ yields

$$\tau_G \geqq \frac{\rho^B - \rho^A + \tau_p}{\tau_p} \tag{10}$$

In this equation, τ_G represents a lower limit on gas transmittance which corresponds to an upper limit on concentration. (See eq. (4).) The determination of τ_G, therefore, requires a knowledge of the opacity $1 - \tau_p$. If separate remote measurements of opacity are not available, an estimate obtained from previous in-stack measurements will usually suffice. Finally, for those cases where no additional data are available, a range of SO_2 levels may be determined for opacities in the range 0 to 20 percent which encompasses the maximum opacity allowed by law for stacks built after August 17, 1971 (ref. 1). For plumes containing few particulates or aerosols (e.g., oil-fired plants), the scattering is insignificant ($\Sigma \approx 0$) so that

$$\tau_G = \rho^B \tag{11}$$

Velocity

Slow motion playback of video-taped plumes exhibit easily discernible fluctuations in the SO_2 concentration. A method of determining the average velocity of the fluctuations was therefore devised by measuring the time of travel t between two fixed points in the scene. Video waveform analyzers were employed to monitor the scene intensity at the two selected points in the plume. A commercial correlation analyzer was then employed to compute the crosscorrelation function of the two signals. The peak of the resulting correlogram gives the desired time (ref. 13). The velocity of the fluctuations is then given by $X/(t \cos \theta)$ where X is the separation of the points in the scene and θ is the viewing angle of the observer.

INSTRUMENTATION

Concentration

A schematic of the system is shown in figure 3. The components shown along the top line are those required for concentration measurements. The camera is outfitted with an ultraviolet (UV) sensitive vidicon tube and a UV lens. Interference filters are used to alternately select the in-band (B) and adjacent (A) spectral channels. These filters have a half-width of approximately 7.5 nm and are centered at 318 nm (B) and 340 nm (A). The video output from the camera is sent to a waveform analyzer which superimposes electronic cross hairs on the scene and also allows a measurement of the scene intensity at the intersection of the cross hairs. This measurement is usually displayed on a digital voltmeter for ease in data reduction. A video timer is also employed to superimpose timing information (month, day, hour, etc.). The resultant composite video signal is displayed on a small monitor and can also be taped for future measurement and reference. Figure 4 shows the system deployed in the field. (The plumes here are invisible.) Figure 5 shows a typical UV scene as photographed from the monitor face. In practice, the background radiance R_3 is an average of two readings taken on either side of the plume. The plume radiance R_2 is measured through the plume center just above the stack lip.

As mentioned earlier, the observer and target are embedded in the scattering medium (source) and, as a result, require a correction for the path radiance between the observer and target. The level of this path radiance is usually small, being of the order of 5 to 10 percent of I_0 at a distance of 400 m. In order to account for this radiance, a large, flat, blackened surface was employed in the field to limit the path, but was unsuitable because of the high intensity of the directly scattered sunlight. A black target utilizing blackbody effects practical for large surface areas was therefore developed. The black target consists of a 40- by 50- by 10-cm section of commercially available aluminum honeycomb, placed in a metal box and mounted on a tripod. The honeycomb material has a cell size of 0.95 cm and presents very little surface area to the observer, the ratio of edge area to honeycomb area being about 3 percent. The inside of the metal box and the honeycomb material were then coated with an optically flat, black paint. The painted surfaces, in conjunction with the blackbody effects of the honeycomb structure, render a black level which is

practically independent of view angle and Sun angle. In practice, the analyzer output is zeroed while looking at the black target at a distance comparable with the observer-plume distance. When used in this manner, no further corrections for path radiance are required.

Velocity

By adding an additional waveform analyzer to the system (lower line of components in fig. 3), the time of travel between two fixed points in the scene can be determined. Figure 6 shows the double cross-hair arrangement employed on a coal-fired stack plume and figure 7 is a dual-beam oscilloscope trace illustrating the appearance of the fluctuations as they pass the upper and lower cross-hair locations shown in figure 6. In order to determine the mean time t that it takes the fluctuations to travel the distance, the two signals are fed to a commercial 400-channel digital correlation analyzer. By taking the crosscorrelation of the two signals, a correlogram is obtained (fig. 8) whose peak gives the desired time (ref. 13). A sampling increment of 0.5 msec is nominally employed and linear averaging is performed for 65 seconds. The crosscorrelation function is then output to an x,y recorder for final analysis. Figure 9 shows a system that was installed in a mobile van for measuring both SO_2 and velocity. This system is more complex than need be, however, since a Fourier transform analyzer (FTA) was included for studying the power spectrum of the fluctuations. The system, as shown, was used in the field. The normal procedure for velocity, however, is to record the data with a system like that shown in figure 4 and analyze the tapes later in the laboratory.

CALIBRATION FOR SO_2

With the sky as a source, calibration of the system was performed using 10.0-cm path length quartz cells filled to selected pressures of SO_2 with nitrogen added to bring the total pressure to 1 atmosphere. The measured transmittance values were corrected for window transmittance and the resultant values plotted as a function of ZL/T (refer to eq. (4)). Such a calibration obtained by using four cells is shown in figure 10. The filter passband employed encompasses several peaks of the SO_2 band system. Deviation from Beer's law is, therefore, expected for this situation in which absorption occurs at different rates across the passband. Interference filter leakage will also cause deviations to occur which tend to compensate for the passband problem. The leakage effect is difficult to assess, particularly in the near wings. In the far wings, although the blocking is good, the integration of a spectrally broad source over a large spectral interval can still produce a nonnegligible impurity. Weak secondary maxima in the filter also exist which enhance this effect. Filtering measurements indicate that approximately 1.5 percent of the sky intensity transmitted through the 318-nm filter originates from light at wavelengths greater than 350 nm. These deviations do not noticeably alter the calibration curve for the transmission range shown and only introduce significant effects at the lower transmittance levels (not shown).

The derivation of equation (4) and the subsequent calibration curve shown in figure 10 assumed that the spectral absorption coefficient was independent of temperature. The temperature factor contained in equation (4) merely reflects the fact that the technique measures density and that the calibration is carried out at ambient temperature. Apart from this density factor, another temperature effect has been observed and referred to as a "temperature broadening" effect (ref. 5). This effect was studied in absorption by use of a deuterium background source and a 2-m Czerny-Turner spectrometer having a resolution of 0.006 nm in the region of the SO_2 band system. Two 10.0-cm-long quartz cells were employed, both loaded to 9.0 torr of SO_2. (1 torr = 133 N/m^2.) Nitrogen was then added to one cell to atmospheric pressure (760 torr) while the other was filled to 535 torr. The spectra of the two cells at ambient temperature were identical, and thus indicates that there are no observable pressure effects at this pressure level. However, when the 535-torr cell was heated to 420 K (identical total pressure of the two cells), a distinct temperature effect can be observed (fig. 11). When heated, most of the peaks in the spectrum decrease in absorption, whereas the valleys increase. A very large correction is, therefore, required for some techniques, such as for differential absorption lidars. For example, the differential absorption coefficient (α(peak) - α(valley)) for the 313-nm peak and adjacent valley (312 nm) changes by 30 percent over this temperature range.

In order to assess the effect of "temperature broadening" on the video technique, the cells were viewed by the system in the standard mode using the sky as a background. In this manner, the integrated effects over the spectral passband of the filter were obtained. The averaged absorption coefficient increased by 8 percent; thus, the measured concentration was required to be decreased by this factor at the 420 K level. This correction was employed in all the stack measurements in this report.

A check of the calibration was made by using a large environmentally controlled tank. The tank was 18.3 m long and 1.83 m in diameter and the longitudinal path is normally used for calibrating pulsed-laser pollution-monitoring systems. The tank has gas manifolds and detection systems for maintaining set levels of pollutant gases. For the SO_2 measurements, a windowless transverse path was employed. The SO_2 concentration was monitored at the center of the tank by a commercial electrochemical analyzer. The tank was located outdoors and the ambient temperature was 298 K so that no temperature corrections were required. The results are shown in figure 12 for the concentration range 500 to 1200 ppm. Good agreement is attained overall. The deviations that do exist are thought to be primarily attributable to ambient wind effects which affect the concentration (hence path length) near the open ports.

PLUME GEOMETRY AND FLOW CONSIDERATIONS

Before considering the results of stack measurements in the field, the pertinent characteristics of free turbulent flow will be considered (ref. 14). Figure 13 illustrates the general character of the near-field flow pattern as exhaust gases come into contact with the stationary ambient field. A potential core region exists in which the velocity and concentration values are given by their stack exit values. This region persists for a distance of several stack

diameters downstream. In addition, a turbulent mixing region is formed between the effluent gases in the core and the ambient air. This mixing region spreads to the center line of the flow where it then comprises the entire flow field. The mixing region also spreads out into the ambient field. The flow regions labeled in figure 13 represent time-averaged values and are never so sharply defined in practice.

Sulfur dioxide concentration is determined from the gas transmittance measured through the center of the plume just above the stack lip. At this point, the major part of the gaseous attenuation comes from the core region (having stack lip concentration Z_0) and the mixing zone effects are small. It is then sufficient to take $L_o/\cos\theta$ (L_o is the stack lip diameter) as the path length through the plume. The transmittance can then be related to ZL/T through the calibration (fig. 10) and the concentration can be inferred if the plume temperature is known. An approximate plume temperature T (K) is usually known for the different classes of stacks and does not play a significant role in the measurement.

Effluent velocity measurements are made by tracking the fluctuations in SO_2 concentration in the plume. Video playback reveals that the edges of the plume are not smooth but exhibit a random distribution of large-scale eddies which propagate downstream through the mixing region. The optical tracking of eddies employed here has a great deal in common with hot-wire anemometer measurements employed earlier (ref. 15) in a laboratory-controlled flow environment to define and measure a convection velocity V_c. In these measurements, pairs of hot wires were used in a crosscorrelation mode to find the time delay corresponding to a given separation of the pair. These laboratory measurements indicate that within a few exit diameters, the eddy convection velocity is roughly constant across the mixing layer and is on the order of one-half the flow velocity in the core. Although flow conditions encountered in the field are expected to be perturbed considerably, these laboratory results, coupled with the flattened radial profiles expected for turbulent tube flow (refs. 7 and 16), suggest that the eddy convection velocity measured in stack plumes will similarly be approximately one-half that of the mean velocity predicted for the core from in-stack measurements. Measurements were, therefore, performed at instrumented stacks to empirically establish this relationship.

Once the concentration and velocity have been measured, the emission rate E (kg/hr) can be determined from

$$E = 2.28 \frac{ZL_o^2V}{T} \tag{12}$$

where Z (ppm) is the SO_2 concentration, L_o (m) is the stack exit diameter, and V (m/s) $\approx 2V_c$ is the velocity inferred from tracking the eddies.

STACK MEASUREMENTS

Tests with the video system have been carried out in cooperation with the EPA at two coal-fired power plants. These tests were conducted by the Special Techniques Group, Emission Measurements and Characterization Division, of the EPA Environmental Science Research Laboratory, as part of their continuing program of evaluation of remote-sensing methods. In these evaluations, in-stack pollutant concentrations and velocities are measured by the appropriate reference methods and also by various continuous monitors. These in-stack measurements provide "ground truth" data with which the remote measurements can be compared. This section will describe the measurement programs at the Riverbend Steam Station, Duke Power Company near Charlotte, North Carolina; at a steam station in the southwestern United States; and at several other facilities.

Riverbend Steam Station

The Riverbend Steam Station is a coal-fired power plant with four boilers. Each boiler drives a turbine generator capable of a maximum output of 150 MW. Each unit is equipped with electrostatic precipitators which remove over 99 percent of the particulates and result in a plume nearly invisible to the eye (Opacity $\approx$ 5 to 10 percent). The effluents of each boiler are divided between two stacks (total of eight stacks for the plant). The stacks are 66 m tall from ground level and each is topped with a converging section designed to increase the effluent velocity for better dispersion. The EPA, with the cooperation of Duke Power Company, has installed a number of ports in one of the stacks at roof level. Figure 4 shows the arrangement of the stacks and figure 5 shows a typical converging section and SO_2 plume.

Tests to determine the ability of the video system to measure effluent velocity were conducted during July 1976. In-stack measurements of the average velocity were made (method 2) at the roof level ports. The constriction at the top of the stack requires that the velocity at the roof level be multiplied by a factor of 2.38 (area factor) to obtain an estimate of the average velocity at the stack lip. Earlier measurements with a remote LDV system consistently gave results 10 to 20 percent lower than those predicted by in-stack measurements (ref. 7). For this reason, a vane velocimeter was also employed in the present tests to measure the center-line velocity at the stack lip. The vane velocimeter is a small, fan-type velocity sensor developed by Langley's flight instrumentation engineers for use on free-falling, aircraft drop models. The sensor consists of a small propeller mounted on the shaft of a precision dc generator, the output voltage of which is proportional to the air velocity (rotational speed of the fan).

The effluent velocity in the stack has been shown to be a linear function of the power load (ref. 7). A scheduled sequence of four power load levels was, therefore, performed in order to test the ability of the video system to track the effluent velocity. Correlograms obtained at the four load levels are shown in figure 14. These correlograms were obtained with measurement points (cross hairs) separated by 1 meter in the flow and positioned along the center line of the plume. Better contrast of the eddies could be obtained near the edge of the plume, but this region is not generally used because of possible

shifts in the plume position as a result of the ambient wind field. A comparison of the various velocity measurements is shown in figure 15. The hatched areas show the range of measurements made earlier with in-stack pitot tubes and a remote LDV system (ref. 7). These measurements illustrate the linear relationship which exists between the plant output in megawatts and the effluent velocity. Pitot tube measurements taken simultaneously with the present video tests are also shown (open circles). Pitot tube, video, and vane velocimeter measurements were made simultaneously at the 125-MW level on a different day. The video measurements of velocity (solid points) are seen to properly track the load. (In-stack SO_2 concentration was steady during the power changes averaging 1190 ppm.) The vane velocimeter result is about 20 percent lower than that predicted from in-stack pitot tube measurements, which is in general agreement with the earlier LDV measurements. These results, coupled with a large asymmetry observed in the in-stack velocity distribution (possibly because of the proximity of stack fans and a 90° turn in the flow direction), suggest that the simple 2.38 area factor applied to account for the converging section may not be sufficient to describe the true velocity conditions. For these reasons, and in light of results to be presented in the next section, an empirical factor of 2.3 was chosen to represent the ratio of the average flow velocity to the convection velocity.

Immediately following the power level changes mentioned above, the power level was held at 130 MW and several precipitator banks were deenergized in order to assess the effects of increased particulate opacity on the SO_2 measurements. The opacity was determined from an in-stack transmissometer corrected to yield stack lip opacity. The results are shown in table I where the opacity increased from a normal value of 8 percent to 21 percent. The SO_2 concentration obtained by using equation (10) differs very little from the values obtained by using $\tau_G = \rho^B$ (eq. (11)) directly. For this case, the particulate scattering effects just compensate for the increased attenuation due to the particulates.

TABLE I.- EFFECT OF OPACITY $(1 - \tau_p)$ ON SO_2 CONCENTRATION MEASUREMENTS AT THE RIVERBEND POWER STATION

[Measurements taken 7/21/76; slant range was 170 m]

Power output, MW	Opacity, percent	ρ^B	ρ^A	Z (eq. (10)), ppm	Z (eq. (11)), ppm	Z (method 6), ppm
130	8	0.66	0.97	990	990	1210
130	21	.64	.92	1040	1070	1170

As mentioned earlier, the path radiance between the observer and the target renders the concentration as a function of range. The black target was employed at the Riverbend plant in an attempt to suppress this effect. The

generator output was held steady at 130 MW for these tests. The remote video measurements were taken along a premarked road leading away from the plant and the black target was located at a point on the road equivalent to the observer-stack lip distance. The results of these measurements are shown in figure 16 for a slant range of 120 to 560 m. The observed concentration is still seen to decrease considerably with increasing range. Part of this decrease is believed to be a result of the finite spatial resolution of the instrument and the decreasing image size, which forces the measurements to be taken at higher positions in the plume. The concentration in the mixing zone continually decreases in the downstream direction because of the influx of the ambient air, whereas the increased path length only partially compensates for this concentration decrease. Thus, it is believed that many remote techniques will exhibit ranging effects due to spatial resolution and plume geometry considerations. In this regard, it should be noted that the video technique has a unique capability for making refinements in these plume geometry effects if desired. Finally, it should be mentioned that measurements have also been made at a slant range of 1300 m. At this extreme range, measurements are considerably inaccurate. The visualization obtained, however, should be particularly valuable for qualitatively studying plume dispersal and wind effects.

Southwestern United States Steam Station

Tests were also conducted at a steam station located in the southwestern part of the United States. The plant selected by the EPA for these tests has only a single stack which is desirable for comparing remote perimeter measurements with in-stack measurements. The plant is a coal-fired, base line station which operates at a fixed output of approximately 350 MW. The single stack is 120 m in height from ground level and has a slight taper in going from a 6.7-m I.D. at the lower port level to 6.1-m I.D. at the stack lip. In-stack SO_2 concentration measurements were made at the ports by using method 6 procedures and also with a permanently installed, commercially available instrument based on an ultraviolet absorption technique. An in-stack transmissometer provided opacity data during the tests. The opacity ranges between 10 and 20 percent with occasional bursts to 25 or 30 percent due to soot blowing of the air preheaters. Effluent velocity was measured in the stack by method 2 and a small correction (1.21) for the stack taper was applied to yield the stack exit velocity. The in-stack velocity measurements at this plant exhibit a far better uniformity than previously observed at the Riverbend plant. At this plant, a typical mean exit velocity (method 2) was determined to be 22.4 m/sec with a standard deviation of 1.4 m/sec. A remote LDV system was also employed at this site to measure the exit velocity directly (ref. 17).

The video system was located at a slant range of approximately 400 m from the stack lip. The ranging problems associated with spatial resolution and plume geometry are not critical at this range, however, because of the large exit diameter (6.1-m I.D.). The black target could not conveniently be placed at a comparable observer-stack lip distance, so it was placed in the foreground at about one-third the distance to the stack lip. The path radiance for this short path was then measured, tripled, and subtracted from each of the measured radiances R_2 and R_3. The results of concentration and velocity measurements performed on August 3 and 4, 1976, are shown in table II. The video concentra-

tion measurements were determined from equation (10) by using an assumed opacity of 15 percent. The plume and sky conditions encountered here, however, exhibit a strong dependence on the assumed opacity. For example, assuming opacity levels of 10 and 20 percent results in concentration levels which differ by -100 and +100 ppm, respectively, from that calculated at the 15-percent level. The reason for the low levels recorded on the in-stack UV system is unknown, but it is interesting to note that this is approximately the same level predicted by the video system if no correction for opacity is made $(\tau_G = \rho^B)$.

TABLE II.- COMPARISON OF SO_2 CONCENTRATION AND EFFLUENT VELOCITY MEASUREMENTS AT THE SOUTHWESTERN UNITED STATES STEAM STATION

Date	Concentration, ppm			Velocity, m/sec		
	Video	UV (in-stack)	Method 6	Video	LDV	Method 2
8/3/76	790	650	740	22.8	----	22.7
8/4/76	860	660	840	21.6	19.1	22.4

Based on the in-stack velocity data obtained at this site, an empirical ratio between the mean velocity and the eddy convection velocity was determined to be 2.3. The agreement between the in-stack measurements and those made by the video system are, therefore, exact and one should look to other measurements using this empirical factor in order to assess its applicability. The LDV measurement is 15 percent lower than that predicted from in-stack measurements. The result is similar to that observed for the LDV measurements at the Riverbend plant and it is not clear whether there is any systematic error involved.

OTHER PLANT EFFLUENTS

The video system has been applied to the measurement of SO_2 concentration and velocity in an oil-fired steam plant and at a sulfuric acid plant. In these facilities, the TV results and associated spectrometer scans indicate that the technique will also be applicable here. No comparisons could be made, however, since no in-stack instrumentation was available at either location. The flow at these plants is considerably slower than that encountered at the large coal-fired plants and appears to have large asymmetries and to be easily affected by the ambient wind conditions. In particular, poor dispersal is observed, including occasional downwash situations. The TV technique is particularly suited for remote measurements under these conditions, since the operator can ascertain the optimum time for measurements when a reasonably stable plume is attained. The use of other remote methods, not having a visualization capability, would be severely hampered in determining the effects of poor plume dispersal and the resultant uncertainty in the optical path length.

These path-length uncertainties greatly overshadow the other instrumental uncertainties, such as stability and calibration errors, normally important to accurate remote measurements.

One additional facility was investigated for application of the video technique. This test involved a garbage incinerator in Newport News, Virginia. The incinerator stack was 53 m high and 3.4-m I.D. at the stack lip. In-stack measurements of velocity were performed by the EPA on March 24, 1976. The video system tracked opacity fluctuations at this site since no appreciable amounts of SO_2 are present in incinerator effluents. The mean velocity measured in the stack was 15.3 m/sec, whereas the video system predicted a velocity of 17.9 m/sec, based on the 2.3 empirical factor. Thus, the video system measures 17 percent high for this facility. Although the empirical factor 2.3 appears to be usable for this facility also, it should be emphasized that this factor is not intended to be used universally, but that it may be necessary to determine this factor for each class of facility investigated.

CONCLUDING REMARKS

The visualization of the otherwise invisible sulfur dioxide plume has many advantages. Foremost among these is the ability to determine the stability of the plume in terms of the stack exit geometry, velocity of the effluent, and the ambient wind conditions. Variations in the optical path length can thus be properly assessed, whereas this uncertainty in the plume geometry and stability is probably the major source of error for line of sight, nonvisual techniques. The visualization aspect can also be used in a qualitative manner at long range to assess the effects of ambient wind conditions on plume dispersal.

Concentration measurements have been conducted at two coal-fired plants. Measurements made within a range of several hundred meters show a good correlation with in-stack measurements. A "temperature broadening" effect has been analyzed which adds an 8-percent correction to the calibration for typical effluent temperatures ($\approx$420 K). The major limitation to concentration measurements is due to the presence of particulates which both attenuate the background light and scatter other ambient light toward the observer. An additional optical channel is therefore employed adjacent to the SO_2 band in order to assess the effects of the scattered light. The use of this channel, in conjunction with an approximate knowledge of the opacity, enables one to correct for the particulate effects.

Effluent velocity measurements are based on optically tracking the large scale eddies which propagate in the mixing zone. The optical tracking approach was shown to be similar to dual hot-wire anemometer measurements used earlier to define an eddy convection velocity although the conditions encountered in the present field measurements cannot be strictly compared with results obtained in a laboratory flow environment. Tests were performed with the video system at two coal-fired power plants in order to compare the method with in-stack techniques. The ratio of the mean in-stack velocity and eddy convection velocity was empirically determined to be 2.3. Using this factor, measurements at the two power plants and at an incinerator showed good agreement with in-stack determinations. The empirical velocity factor is believed to be applicable for

this class of plants. It may be necessary, however, to determine this factor for each new class of facility investigated. The video technique, therefore, is an attractive method for measuring effluent velocity and is considerably less expensive and less complex than the alternative remote technique (laser doppler velocimetry). Finally, the advantage of measuring, with a single instrument, both the concentration and velocity simultaneously cannot be over-emphasized, since in the final analysis the emission rate is the most important pollution parameter.

Langley Research Center
National Aeronautics and Space Administration
Hampton, VA. 23665
July 25, 1977

REFERENCES

1. Standards of Performance for New Stationary Sources. Fed. Regist., vol. 36, no. 247, pt. II, Dec. 23, 1971, pp. 24876-24895.

2. Nader, John S.; Jaye, Fredric; and Conner, William: Performance Specifications for Stationary-Source Monitoring Systems for Gases and Visible Emissions. EPA-650/2-74-013, U.S. Environ. Prot. Agency, Jan. 1975. (Available from NTIS as PB 230 934.)

3. Cook, Charles S.; Bethke, George W.; and Conner, William D.: Remote Measurement of Smoke Plume Transmittance Using Lidar. Appl. Opt., vol. 11, no. 8, Aug. 1972, pp. 1742-1748.

4. Barnes, H. M., Jr.; Herget, W. F.; and Rollins, R.: Remote Sensing of SO_2 in Power Plant Plumes Using Ultraviolet Absorption and Infrared Emission Spectroscopy. Analytical Methods Applied to Air Pollution Measurements, Robert K. Stevens and William F. Herget, eds., Ann Arbor Sci. Publ., Inc., c.1974, pp. 245-266.

5. Moffat, Andrew J.; and Millan, Millan M.: The Applications of Optical Correlation Techniques to the Remote Sensing of SO_2 Plumes Using Sky Light. Atmos. Environ., vol. 5, no. 8, Aug. 1971, pp. 677-690.

6. Wright, M. L.; Proctor, E. K.; Gasiorek, L. S.; and Liston, E. M.: A Preliminary Study of Air-Pollution Measurement by Active Remote-Sensing. NASA CR-132724, 1975.

7. Miller, C. R.; and Sonnenschein, C. M.: Remote Measurement of Power Plant Smoke Stack Effluent Velocity. EPA-650/2-75-062, U.S. Environ. Prot. Agency, Aug. 1975. (Available from NTIS as PB 245 792.)

8. Exton, Reginald J.; and Gregory, Ray W.: A Four-Channel Portable Solar Radiometer for Measuring Particulate and/or Aerosol Opacity and Concentration of NO_2 and SO_2 in Stack Plumes. NASA TN D-8182, 1976.

9. Cutchis, Pythagoras: Stratospheric Ozone Depletion and Solar Ultraviolet Radiation on Earth. Science, vol. 184, no. 4132, Apr. 5, 1974, pp. 13-19.

10. Conner, William D.: Measurement of the Opacity and Mass Concentration of Particulate Emissions by Transmissometry. EPA-650/2-74-128, Nov. 1974.

11. Hall, T. C., Jr.; and Blacet, F. E.: Separation of the Absorption Spectra of NO_2 and N_2O_4 in the Range of 2400-5000 A. J. Chem. Phys., vol. 20, no. 11, Nov. 1952, pp. 1745-1749.

12. Sidebottom, Howard W.; Badcock, Charles C.; Jackson, George E.; Calvert, Jack G.; Reinhardt, George W.; and Damon, Edward K.: Photooxidation of Sulfur Dioxide. Environ. Sci. & Technol., vol. 6, no. 1, Jan. 1972, pp. 72-79.

13. Bendat, Julius S.; and Piersol, Allan G.: Random Data: Analysis and Measurement Procedures. John Wiley & Sons, Inc., c.1971.

14. O'Connor, T. J.; Comfort, E. H.; and Cass, L. A.: Turbulent Mixing of an Axisymmetric Jet of Partially Dissociated Nitrogen With Ambient Air. AIAA J., vol. 4, no. 11, Nov. 1966, pp. 2026-2032.

15. Davies, P. O. A. L.; Fisher, M. J.; and Barratt, M. J.: The Characteristics of the Turbulence in the Mixing Region of a Round Jet. J. Fluid Mech., vol. 15, pt. 3, Mar. 1963, pp. 337-367.

16. Bird, R. Byron; Stewart, Warren E.; and Lightfoot, Edwin N.: Transport Phenomena. John Wiley & Sons, Inc., c.1960.

17. Krause, M. C.; Miller, G. M.; and Gorzynski, E. J.: Evaluation of LDV Techniques for Remote Wind Velocity Measurements. LMSC-HREC TR D497061, Lockheed Missiles & Space Co., Inc., Oct. 1976.

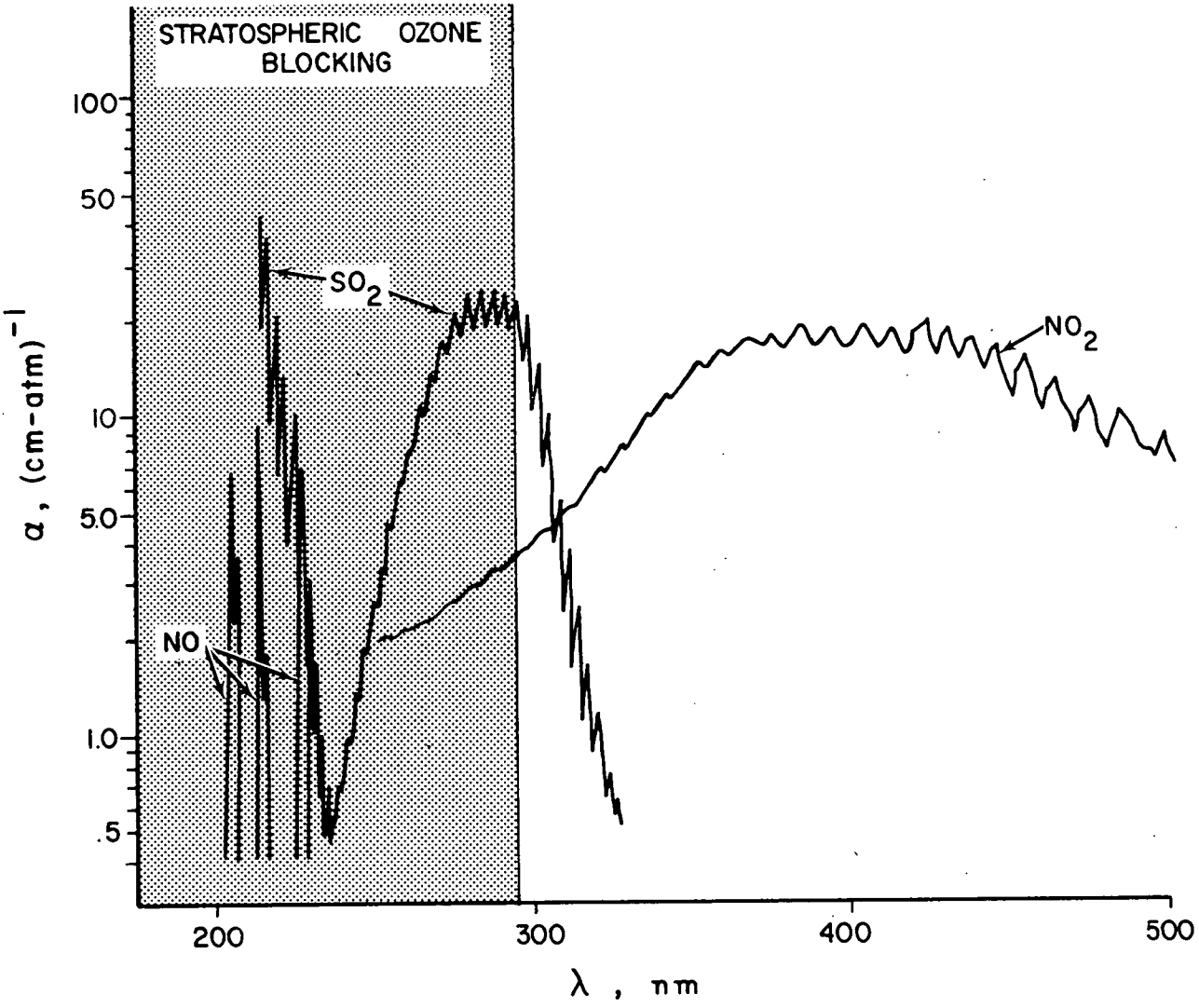

Figure 1.- Spectral absorption coefficients for the gaseous effluents NO, NO_2, and SO_2.

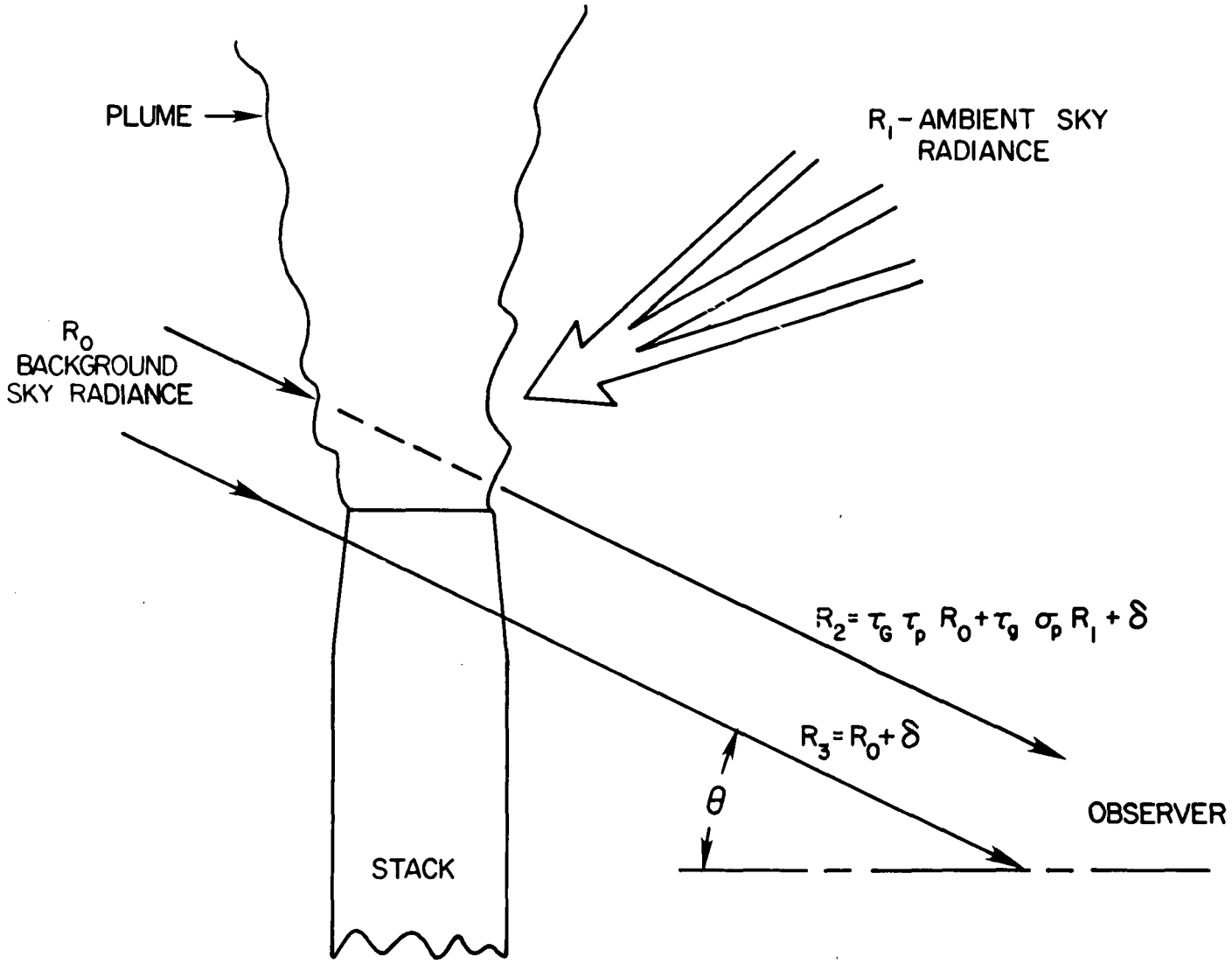

Figure 2.- Contributions to the plume radiance as seen by the observer.

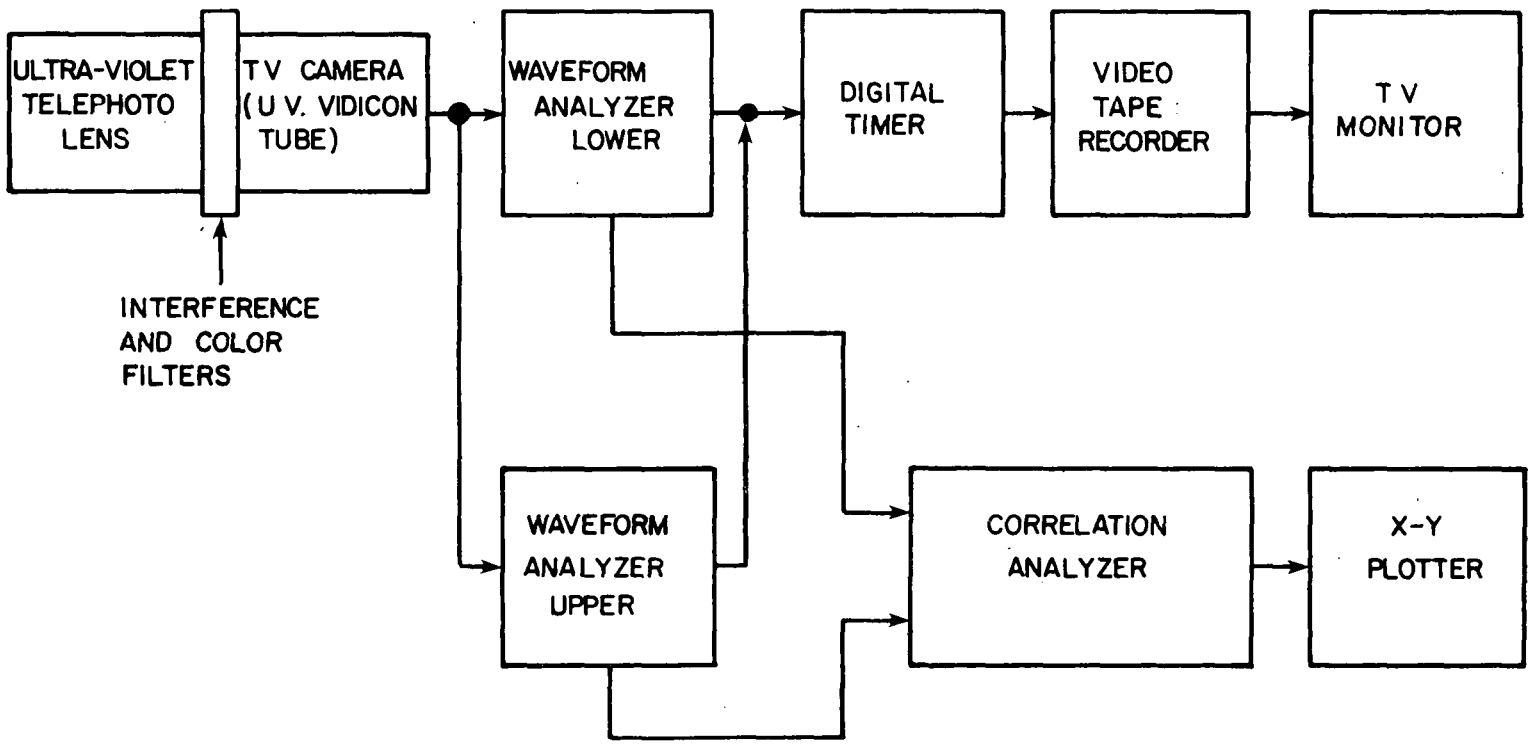

Figure 3.- Schematic of video system. The upper components are those required for concentration measurements. The lower line of components is added to make effluent velocity measurements.

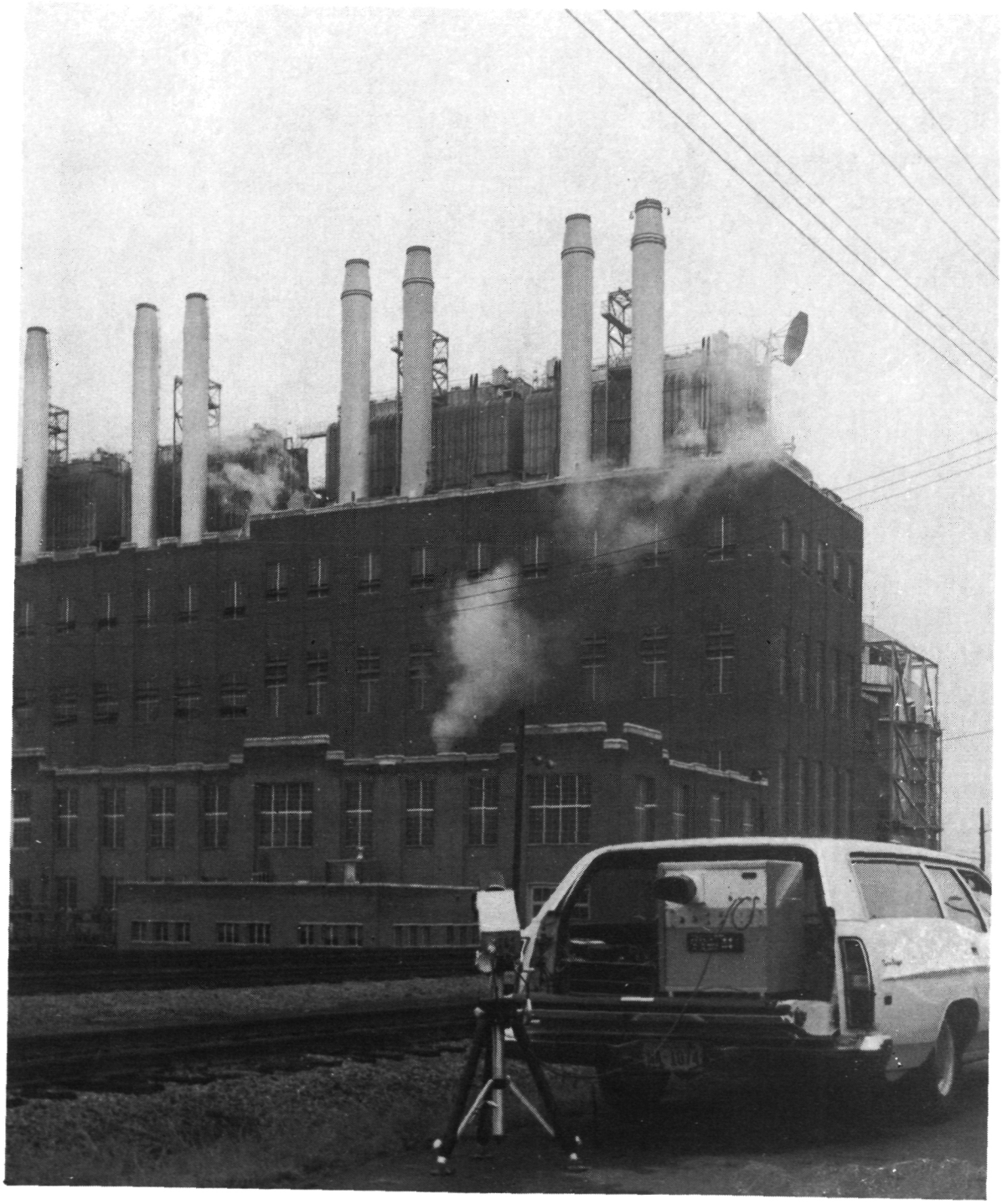

L-74-4704

Figure 4.- Video system deployed in the field. The plumes here are not visible to the eye.

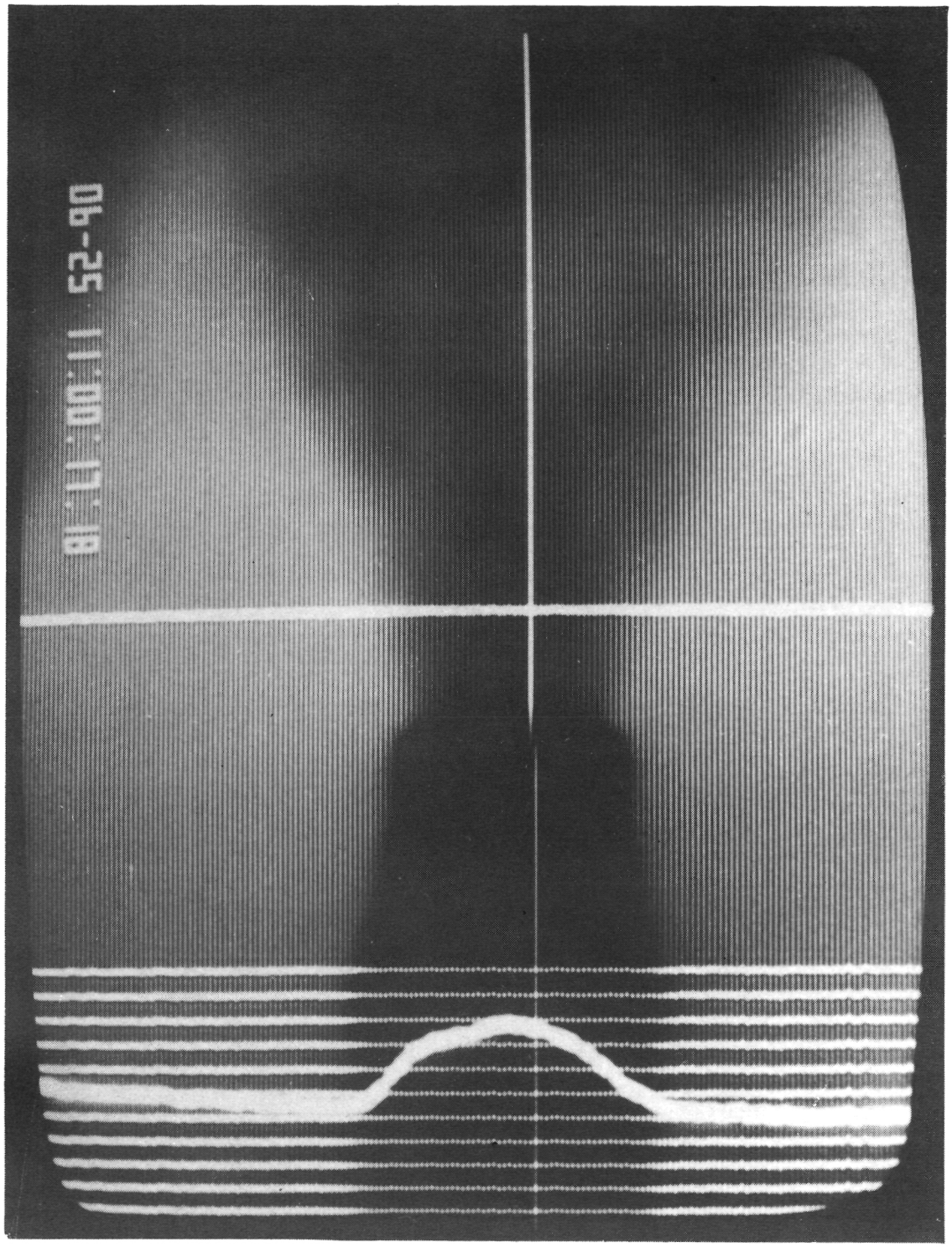

L-74-4292

Figure 5.- A typical stack plume (SO_2 visualization) as photographed from the monitor face. The lower trace is a superimposed display of the intensity along the horizontal cross hair.

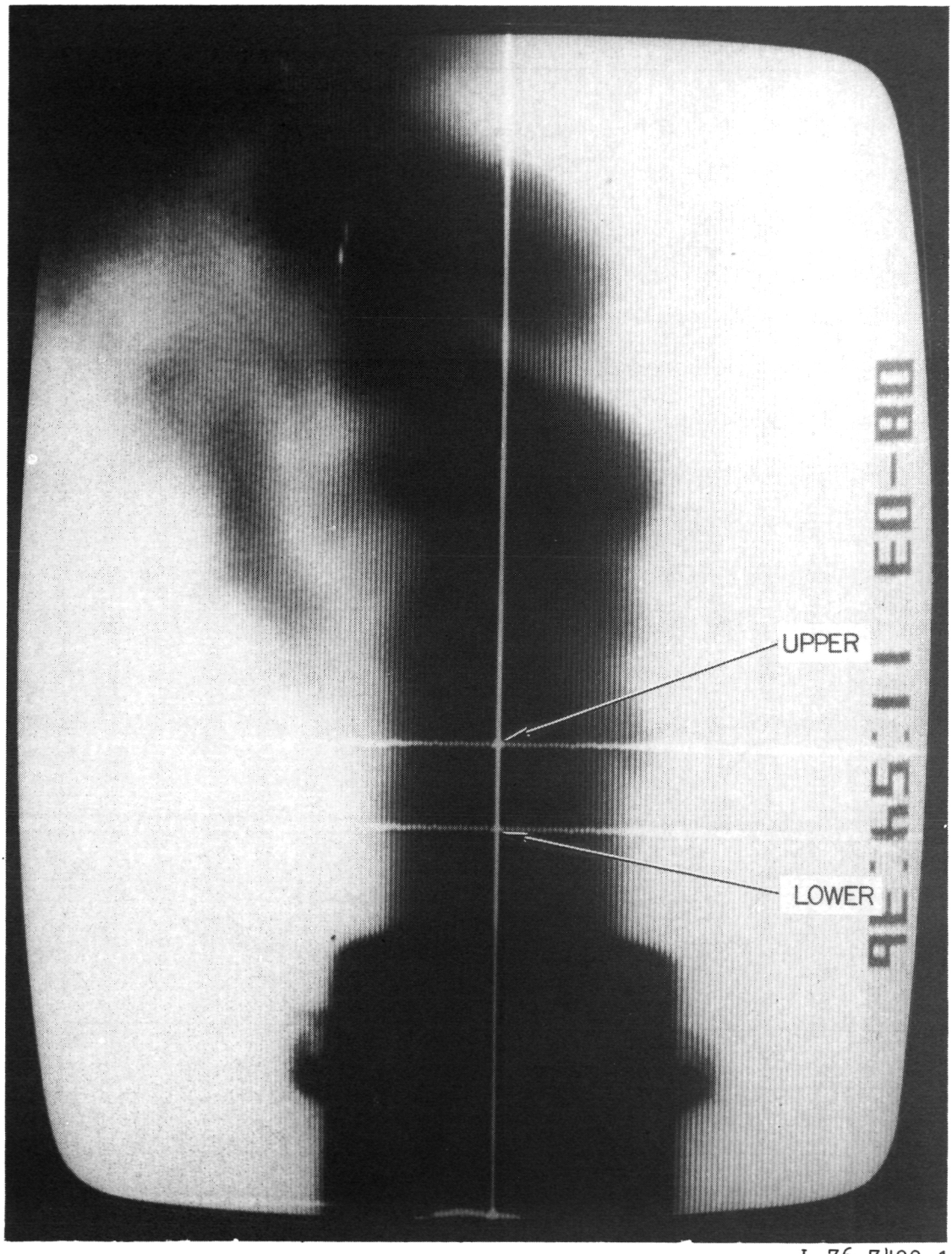

L-76-7499.1

Figure 6.- A double cross-hair arrangement is shown for making effluent velocity measurements.

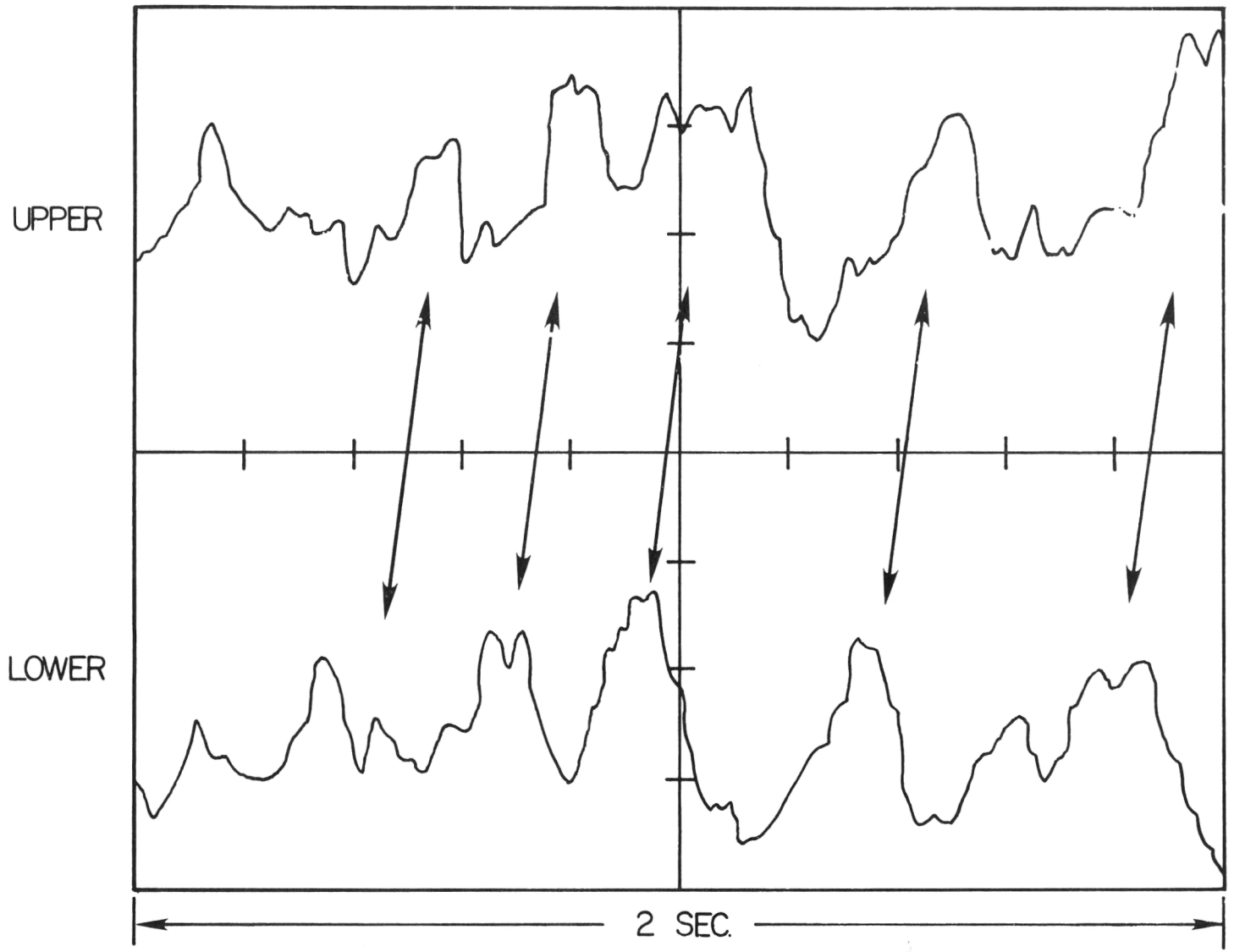

Figure 7.- A dual-beam oscilloscope display illustrating the appearance of the random fluctuations as they pass the two cross-hair locations shown in figure 6. The signals were filtered (20 Hz cutoff) to suppress the video field (frame) rate.

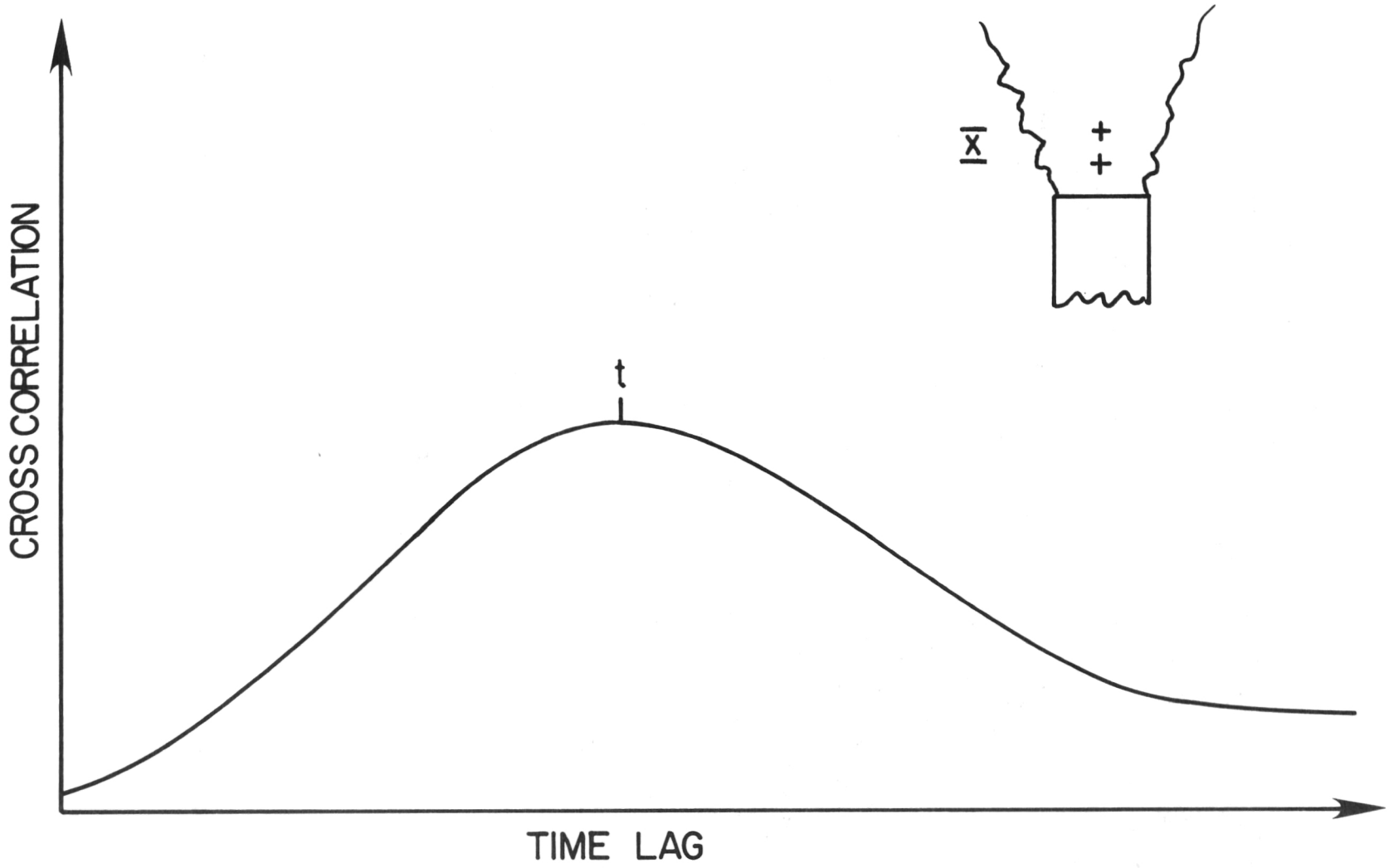

Figure 8.- A typical cross-correlogram. The peak of this function gives the mean time for a fluctuation to traverse the distance between the cross hairs.

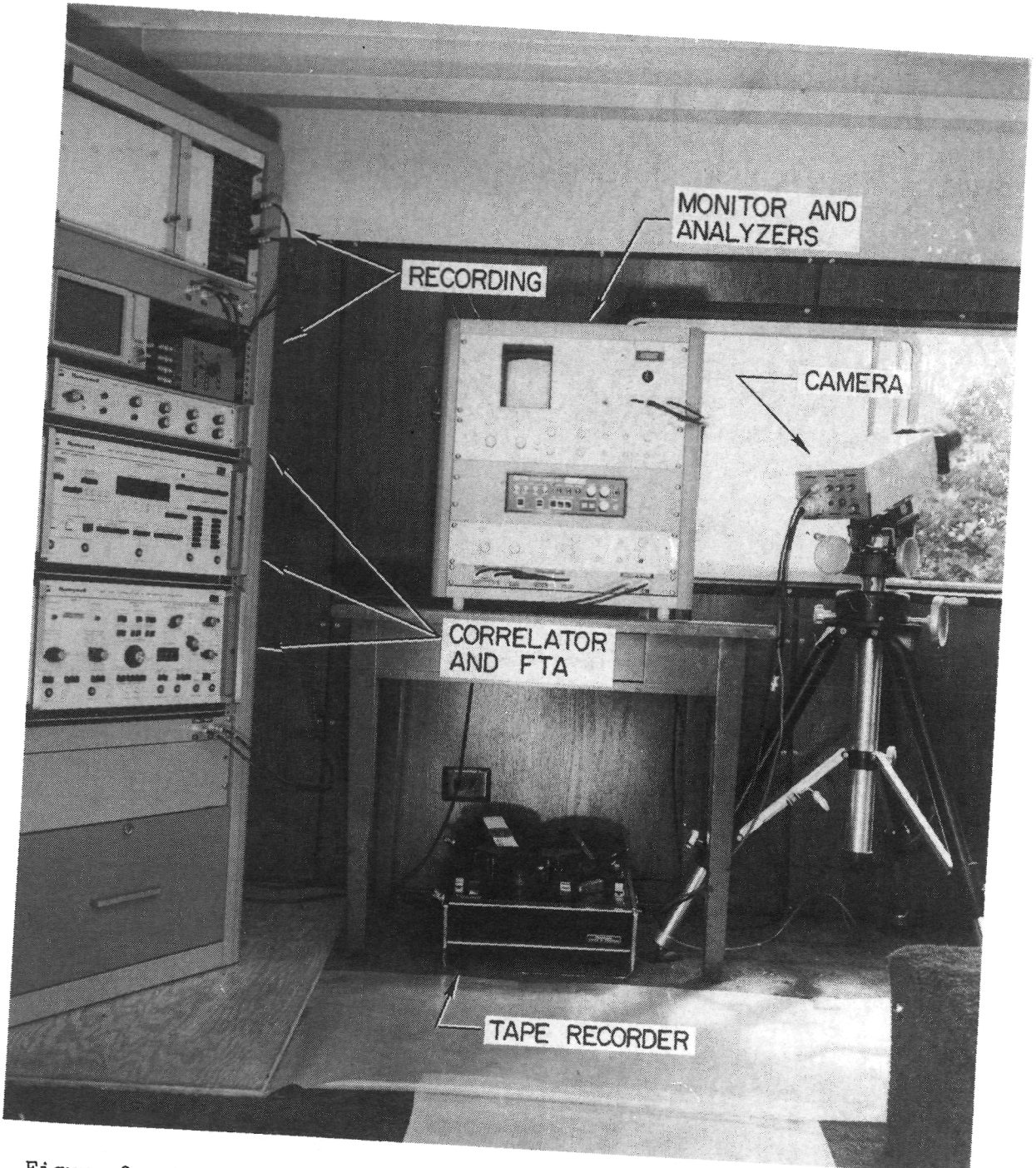

Figure 9.- Video system for measuring both concentration and effluent velocity is shown installed in a mobile van. L-75-6745.1

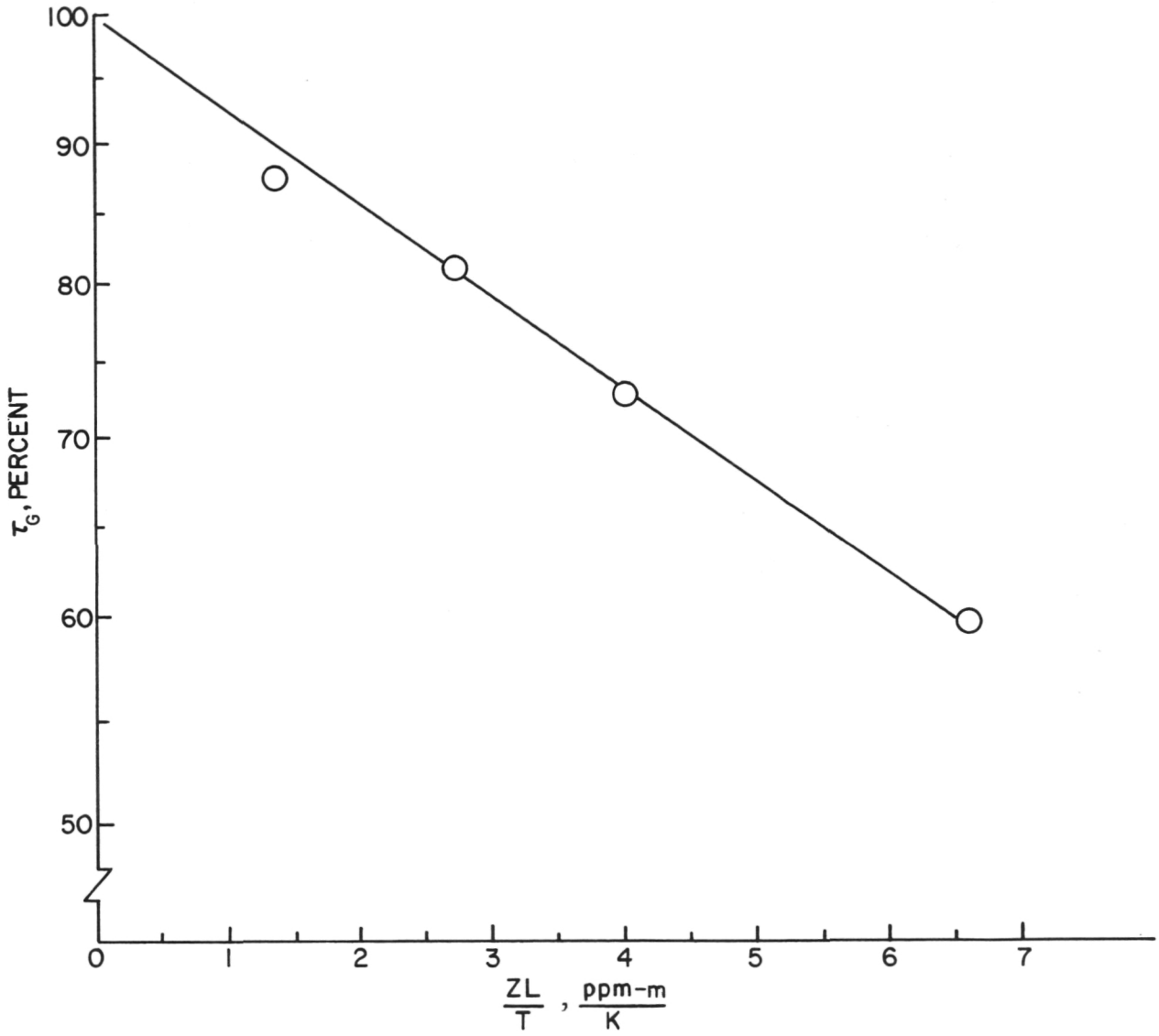

Figure 10.- Calibration curve for SO_2 showing $\ln \tau_G$ plotted against ZL/T.

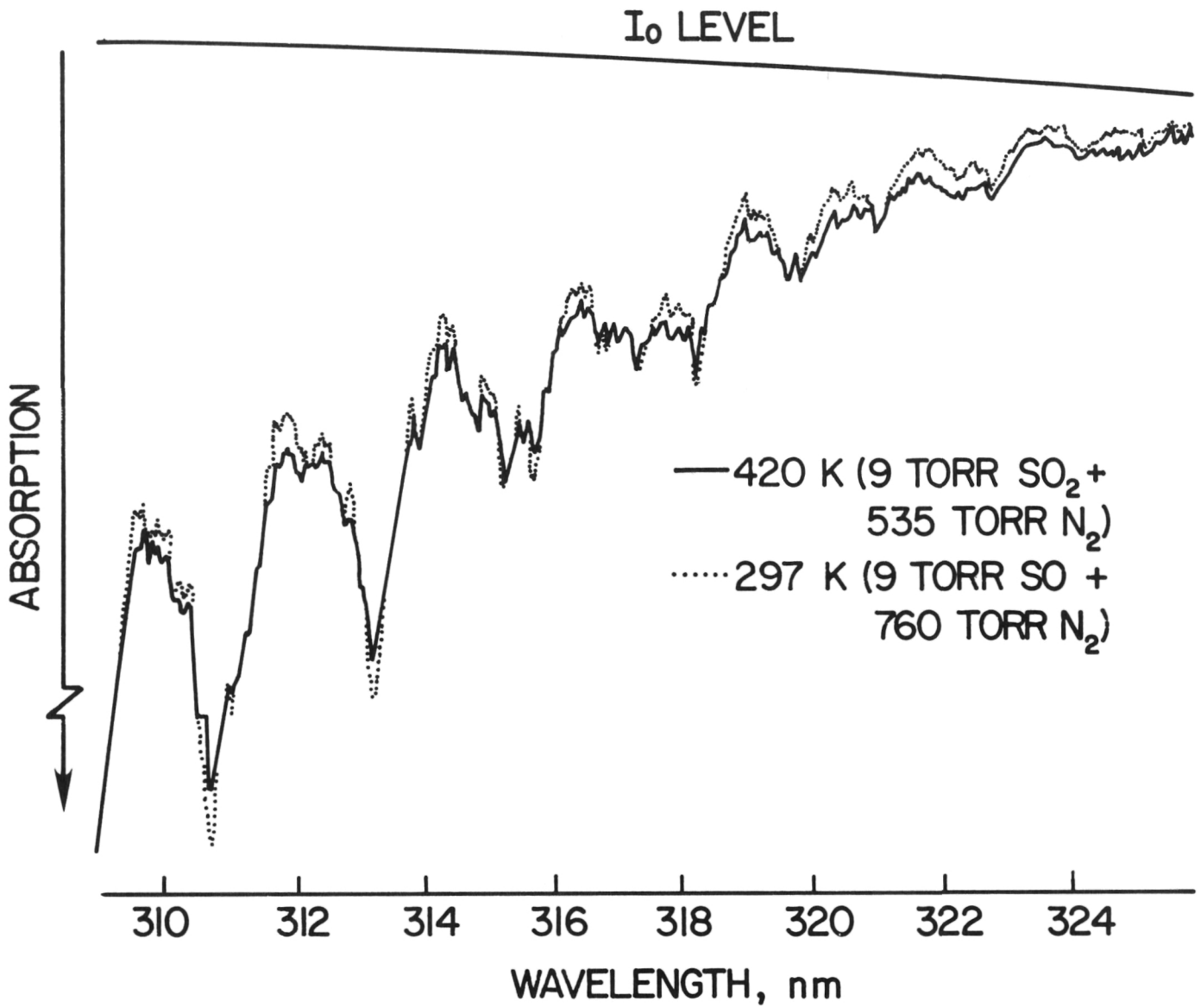

Figure 11.- Absorption spectrum of SO_2 for two temperature settings, 298 K and 420 K.

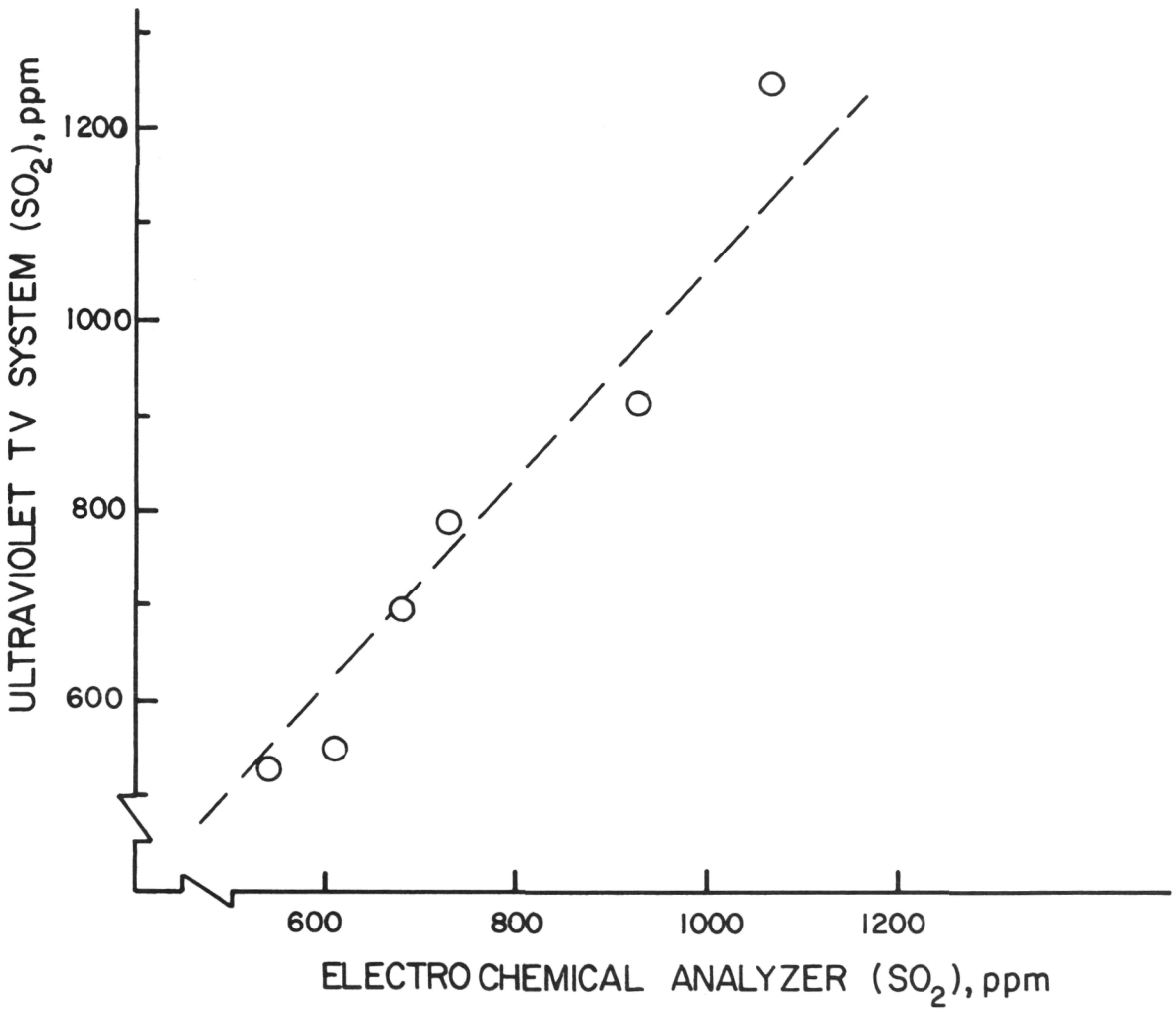

Figure 12.- Calibration check in an environmentally controlled tank.

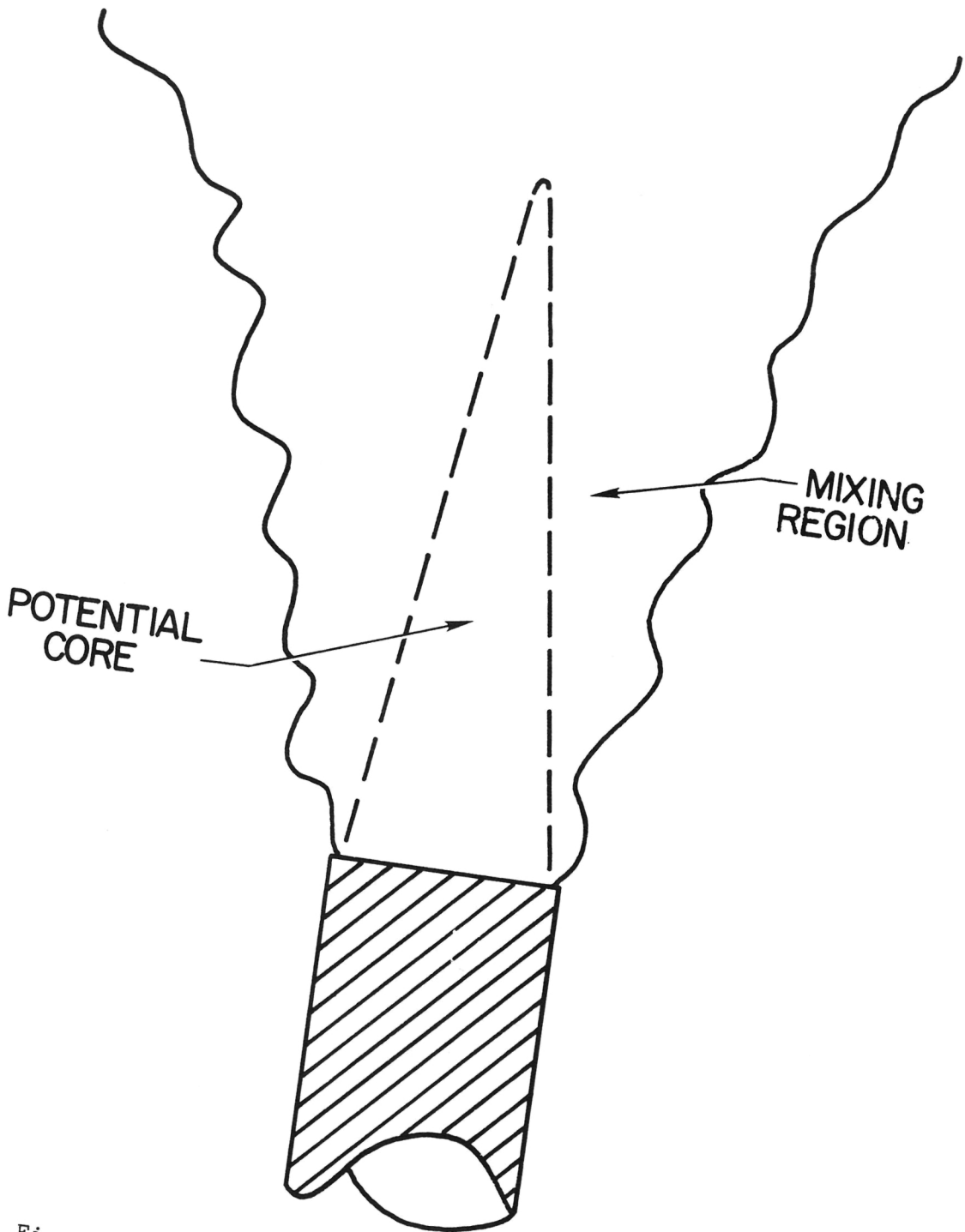

Figure 13.- Characteristics of free turbulent flow.

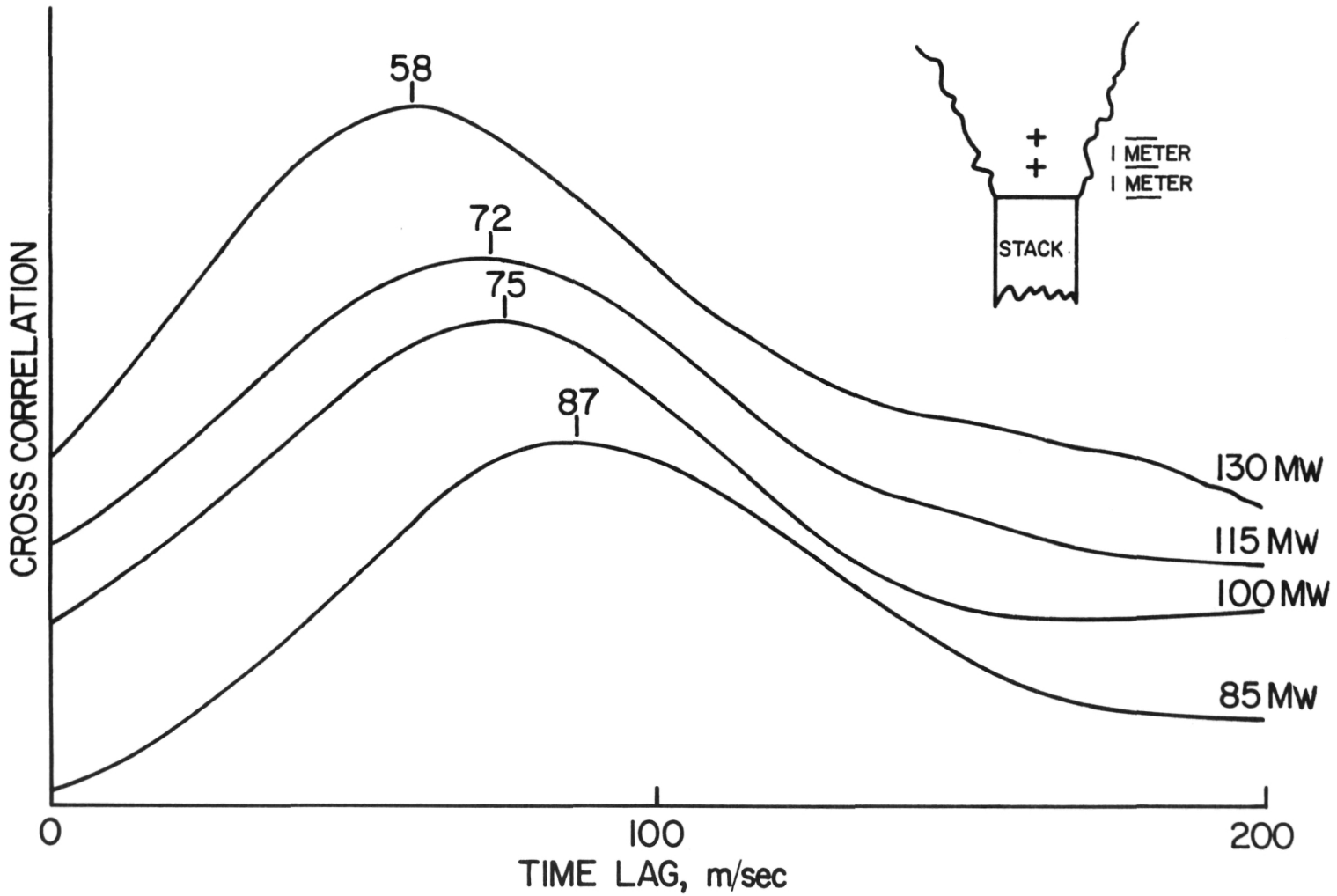

Figure 14.- Cross-correlograms obtained at Riverbend Power Station for a preprogramed sequence of four set power levels (7/21/76). The separation between the video sensing points was 1 meter with the lower point 1 meter above the stack lip.

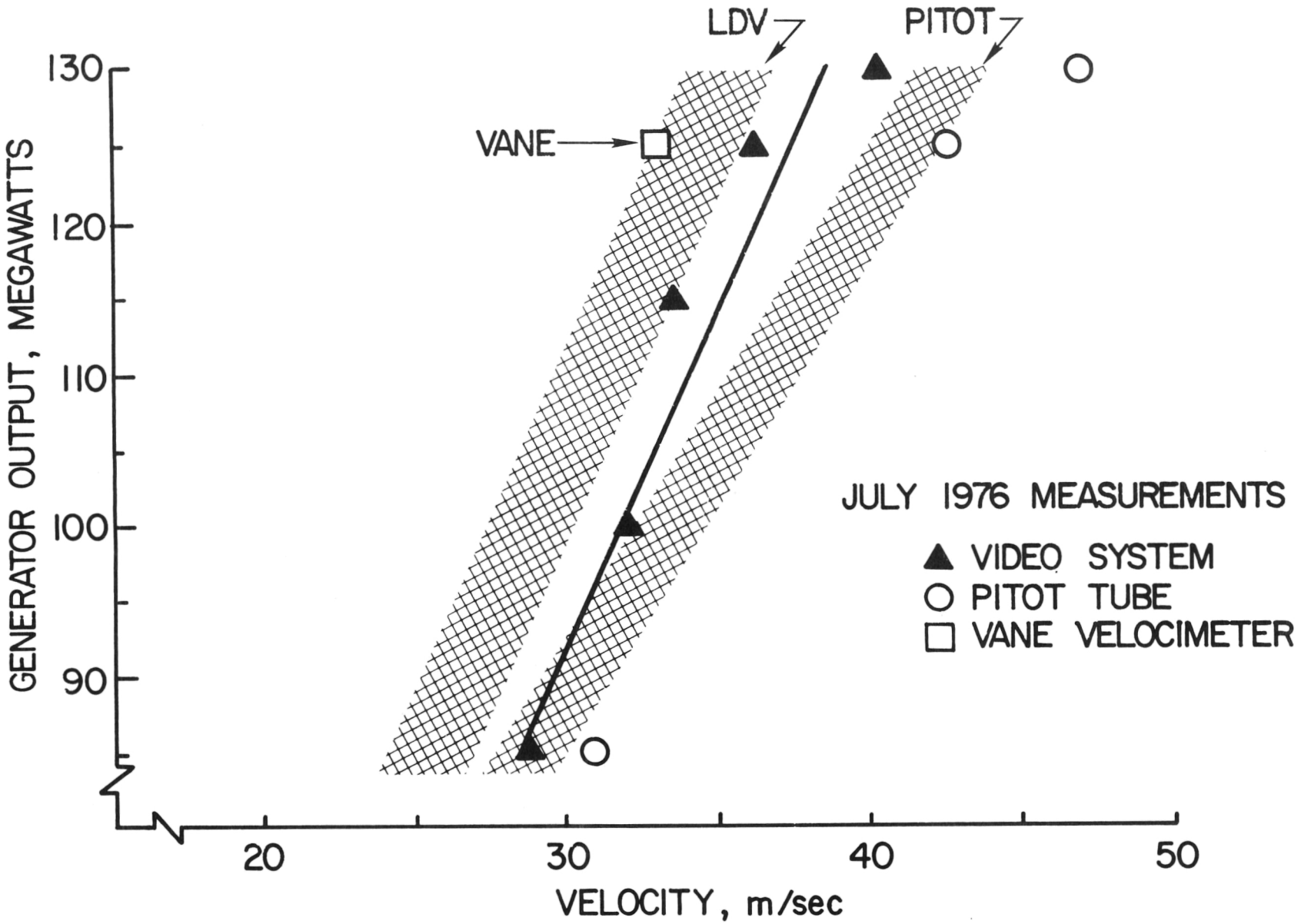

Figure 15.- A comparison of effluent velocity measurements made at the Riverbend Power Station.

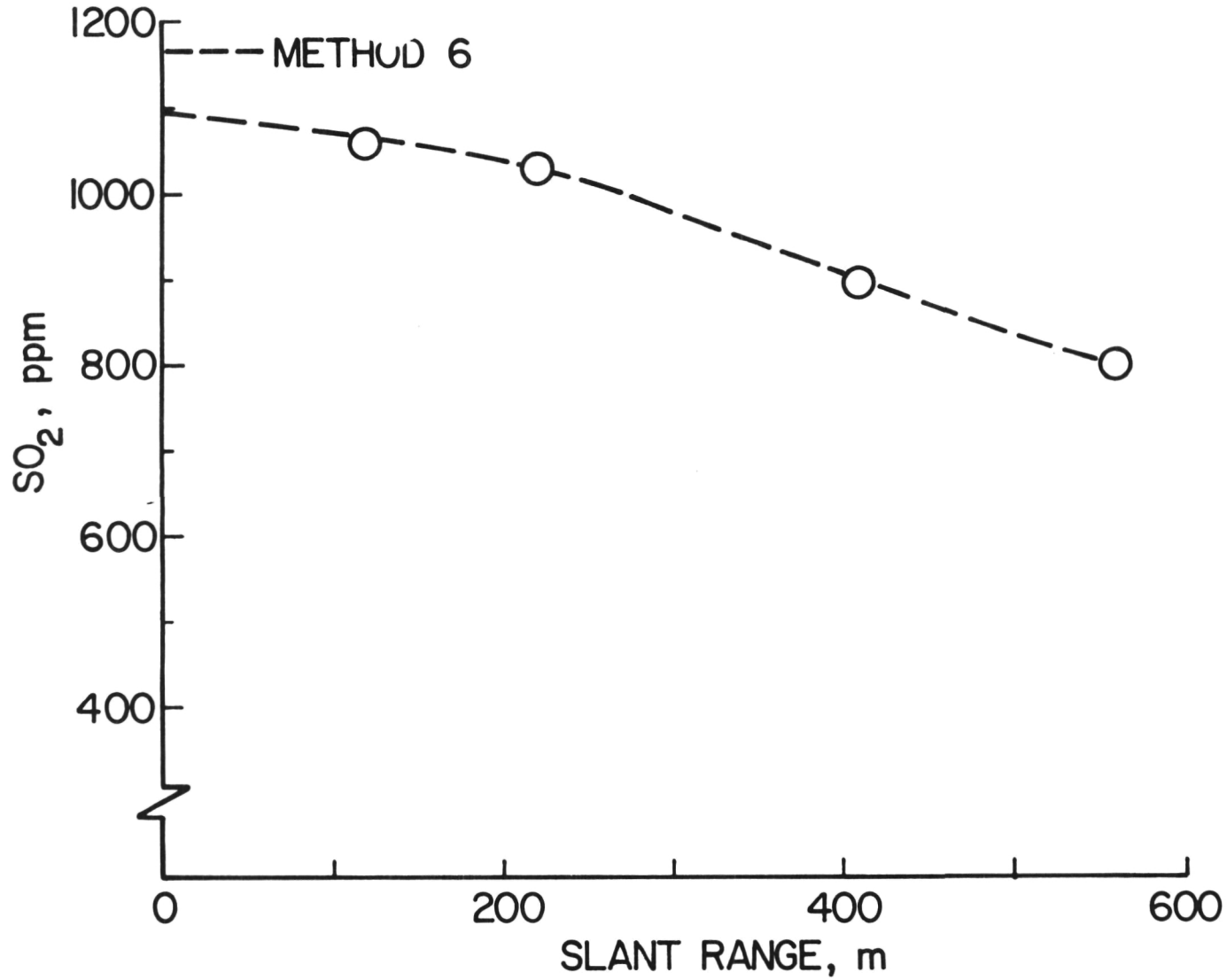

Figure 16.- Effect of range on concentration measurements. A large contribution to this effect is believed to be a result of the finite spatial resolution of the instrument and the decreasing image size, which forces the measurements to be taken at higher positions in the plume (lower ppm-m levels).

1. Report No.	2. Government Accession No.	3. Recipient's Catalog No.
NASA TP-1014		

4. Title and Subtitle	5. Report Date
AN ULTRAVIOLET VIDEO TECHNIQUE FOR VISUALIZATION OF STACK PLUMES AND FOR MEASURING SULFUR DIOXIDE CONCENTRATION AND EFFLUENT VELOCITY	September 1977
	6. Performing Organization Code

7. Author(s)	8. Performing Organization Report No.
Reginald J. Exton	L-11628
	10. Work Unit No. 506-18-12-02
9. Performing Organization Name and Address	11. Contract or Grant No.
NASA Langley Research Center Hampton, VA 23665	
	13. Type of Report and Period Covered
12. Sponsoring Agency Name and Address	Technical Paper
National Aeronautics and Space Administration Washington, DC 20546	14. Sponsoring Agency Code

15. Supplementary Notes

16. Abstract

Absorption spectroscopy utilizing a video sensing technique has been investigated as a means of visualizing SO_2 in power plant stack plumes and for measuring SO_2 concentration and effluent velocity in these plumes. The absorption of SO_2 is measured in the ultraviolet region by using the sky (scattered sunlight) as a background source. An additional spectral channel, adjacent to the SO_2 band system, is used to correct for particulate scattering encountered in coal-fired power plant plumes. The video system also tracks fluctuations in the SO_2 concentration which leads to the determination of an eddy convection velocity. Field measurements were performed to show that the eddy convection velocity is proportional to the average in-stack velocity and to empirically determine their relationship. It was concluded that the video absorption technique is an attractive method for remotely determining both SO_2 concentration and plume velocity with the same instrument.

17. Key Words (Suggested by Author(s))	18. Distribution Statement
Pollution Environmental monitoring Sulfur dioxide	Unclassified - Unlimited Subject Category 45

19. Security Classif. (of this report)	20. Security Classif. (of this page)	21. No. of Pages	22. Price*
Unclassified	Unclassified	35	$4.00

* For sale by the National Technical Information Service, Springfield, Virginia 22161

NASA-Langley, 1977

National Aeronautics and
Space Administration

Washington, D.C.
20546

Official Business
Penalty for Private Use, $300

THIRD-CLASS BULK RATE

Postage and Fees Paid
National Aeronautics and
Space Administration
NASA-451

NASA

POSTMASTER: If Undeliverable (Section 158
Postal Manual) Do Not Return